Modeling of Turbulent Spray Combustion under Cryogenic and Elevated Pressure Conditions

D. SCHLOTZ, M. VOGELGESANG, E. GUTHEIL*
Interdisziplinäres Zentrum für Wissenschaftliches Rechnen, Universität Heidelberg, Im Neuenheimer Feld 368, 69120 Heidelberg, Germany

W. CLAUSS, J. SENDER
DLR Lampoldshausen, Raumfahrtantriebe, Langer Grund, 74239 Hardthausen, Germany

Keywords: Turbulent Spray Combustion, Cryogenic Temperature, CARS, Droplet Tracking Velocimetry, Flamelet Model, Liquid Oxygen

Abbreviated Title: Turbulent Spray Combustion for Liquid Rocket Propulsion

ABSTRACT

The paper concerns both the numerical and experimental investigation of turbulent liquid oxygen/hydrogen spray combustion for elevated subcritical pressure and cryogenic inlet temperature conditions. In particular, the combustion in the single injector combustion chamber is studied where experimental data are obtained for gas phase temperature and both droplet size and velocities. The model uses an Eulerian–Lagrangian formulation for the gas and the liquid phase, respectively. Detailed models for droplet heating and vaporization in a convective flow field are employed, and detailed gas phase reactions are accounted for through use of a flamelet model for turbulent spray combustion. The results show a very good agreement between experimental and computational spray characteristics. The computed gas phase temperature lies somewhat above the experimental values which is associated with CARS single shot measurements and incomplete data for the initial conditions of the combustion process.

INTRODUCTION

An improved understanding of the physical and chemical processes occurring in liquid rocket engines is required to ensure the stability, reliability, and efficiency of their performance. The gaseous hydrogen and the liquid oxygen (LOX) are injected at cryogenic inlet temperatures,

*Correspondig Author

and the turbulent combustion occurs in both the sub- and supercritical domain. Therefore, the models for the processes in systems such as the Ariane V or the Space Shuttle main engine are very complex. In the present study the combustion process in a single injection combustion chamber is investigated for elevated pressure and cryogenic inlet temperatures. An overview of the current status of experimental techniques for cryogenic conditions is given by Brummund *et al.*, 1995.

For the present simulation, experimental data are obtained for an elevated pressure situation of 0.5 MPa at cryogenic inlet temperatures. Gas temperature as well as droplet size and velocities are measured. An overview on CARS measurement technique in combustion processes is given by Eckbreth (1996). The experimental methods employed here are discussed in the present paper.

The combustion in liquid rocket propulsion typically occurs in the flamelet regime of turbulent combustion (Balakrishnan, 1993) which enables the use of the flamelet model for turbulent spray diffusion flames (Hollmann and Gutheil, 1996 and 1998). Structures of laminar hydrogen/oxygen flames are precalculated at 0.5 MPa and for cryogenic inlet temperature of 100 K for hydrogen (Schlotz and Gutheil, 1999 and 2000), and they are incorporated into the turbulent spray combustion model which allows the computation of all chemical species that are included in the detailed chemical reaction mechanism for the hydrogen/oxygen system that includes 8 reactive species and 38 chemical reactions (Warnatz *et al.*, 1993). The following section presents the experimental data. Then the model is discussed. Special attention is given to the evaluation of initial conditions from the experiment used for the simulation. Results and discussion are followed by a summary and future research in the area.

EXPERIMENTAL SETUP

M3 Micro Combustor Facility

The M3 Micro Combustor is a facility for basic research on cryogenic spray combustion. It comprises a single injector where LOX is injected into the gaseous hydrogen where both have cryogenic inlet conditions.

Using a capacitively cooled, windowed model combustion chamber for short run times of approx. 1 s, the test bench is especially designed to reduce startup transients. The combustion chamber is 60 mm x 60 mm in cross section and 140 mm long. Top and bottom walls have centered windows to allow for laser light sheet applications, both side walls are made of quartz for optical access to the entire combustion chamber. For more details about the facility and the combustor, see Sender *et al.* (1997).

A single coaxial injector with dimensions similar to the HM7B type, but without recess and tapering, was placed in the center of the face plate. The HM7B injector is used in the upper stage of the ARIANE IV. The inner diameter of the LOX post is kept constant at 1 mm. The outer diameter of the injector was 3.6 mm for 0.5 MPa of combustion chamber pressure. The lengths of both the LOX and the hydrogen injector lines exceed 20 diameters to ensure a fully developed turbulent flow profile.

Injection and Runtime Conditions

The mean velocity of the reaction products in the combustion chamber is 15 m/s. The flow conditions and typical non-dimensional parameters such as

Weber number	We	=	$\rho_{H_2} \cdot (\mathsf{v}_{H_2} - \mathsf{v}_{O_2})^2 \mathsf{d}_{O_2} / \sigma_{O_2}$,
Reynolds number	Re	=	$(\rho \cdot \mathsf{v} \cdot \mathsf{d})/\nu$,
momentum ratio	J	=	$(\rho \mathsf{v}^2)_{H_2} / (\rho \mathsf{v}^2)_{O_2}$,
mixture ratio	r_{of}	=	$(\dot{m}_{O_2})/(\dot{m}_{H_2})$, and
velocity ratio	V_{fo}	=	$\mathsf{v}_{H_2}/\mathsf{v}_{O_2}$

for the test case are summarized in Tab. I. Here ρ denotes the gas density, $\dot{m}$ the mass fluxes, v the velocity, and ν the viscosity. All parameters have been calculated using injector exit conditions. The O_2 is liquid and the H_2 gaseous in the above definitions. r_{of} denotes the oxygen/air mixture ratio, and V_{fo} the oxygen/fuel velocity ratio, respectively. The diameter of the liquid injection tube, d_{O_2}, is 1.2 mm, and σ denotes the surface tension of the liquid.

Diagnostics

Droplet Tracking Velocimetry (DTV)

DTV is similar to particle tracking velocimetry that has been widely used in PIV applications with low image densities (Adrian, 1991). In DTV the LOX droplets in the flow are used as tracers. Hence, DTV analyzes the velocity of individual droplets whereas a PIV analysis by autocorrelation yields mean velocities of droplet ensembles. The velocity is determined by recording their position at two times on a single frame. The flow is therefore illuminated twice with pulsed light-sheets. From the displacement of the droplet images and the known time interval between the exposure times the velocity can be determined. The two lasers are triggered by an electronic unit that provides an adjustable time delay for the two laser pulses. For the experiments presented, this delay was chosen to be 7 μs. The light sheet was 4 cm of

width and 500 μm of thickness inside the combustion chamber. The camera shutter was need open for 1/60 s. The light originating from the combustion was blocked by an interference band pass filter transparent only at the laser wavelength.

After background subtraction, contrast enhancement, and edge enhancement the image was thresholded to have only binary grey values. Connected pixels were identified as an individual particle whose position was determined by calculating the center of gravity. The area, A, and perimeter, P, of these droplet images were used to discriminate droplets when the ratio $P/A^{1/2}$ differs more than 40% from that of a sphere. A detailed description on the velocity evaluation scheme is found in Sender *et al.* (1997).

Due to the droplets' inertia, they cannot follow the flow without slip, but the droplets should show the average velocity distribution of the main flow field. The estimated relaxation times $\tau = \rho D^2/(18\eta)$ for droplet diameters of 10 μm and 70 μm are of the order of 1 ms and 50 ms, respectively. Hence, typical relaxation times are clearly longer than the shortest turbulent time scales expected. Since the droplet velocity depends on the droplets mass and on its history in the flow field, no unique flow-field for all the droplets can be expected.

Furthermore the calculated droplet image diameters do not reflect the real values due to the evaluation scheme explained above. Major deviations are introduced due to incomplete illumination by the light sheet of the droplets and the image processing. These facts should be taken into account when the results of experiment and simulation are discussed. At the same time these uncertainties are transfered to the evaluation of initial conditions for the simulation which will be discussed below.

Temperature Measurements by CARS

In recent years, Coherent Anti-Stokes Raman Scattering (CARS) became a standard diagnostic tool in many applications ranging from basis research to applied research like the probing of technical combustion chambers. CARS has been used for non intrusive point-wise thermometry in the micro combustion chamber.

The laser part of the CARS spectrometer consists of a single mode Coherent Inc. Infinity Nd:YAG laser delivering 8 mJ per pulse at 25 Hz repetition rate. Pulse duration was 3 ns. The laser beams, adjusted in diameters and divergences by telescopes, with their pulses overlapped in time to better 0.5 ns, were combined in a vertical plane planar BOXCARS (Smirnov *et al.*, 2000; Clauß *et al.*, 1997) configuration where the red and green beams travel together with the yellow beam separated in parallel by 10 mm. The beams are focused into the probe volume with a 200 mm focal length lens. A two axis translation stage was positioned around the microcombustor to facilitate remotely controlled traversing of the probe volume.

In principle, the excitation of the H_2, H_2O, and O_2 molecules is possible at the same time, but we could not get simultaneous detection because the dispersion of the spectrograph was too high to catch the O_2 molecule. Therefore, detection was limited to simultaneous recording of the CARS signals from H_2 and H_2O.

Three cross sections at distances of 52 mm, 87 mm and 127 mm (see Figs. 2 and 3) from the injector plate were probed at 2.5 mm steps. During a test run of 2 s, 50 spectra were recorded with the CARS system running at 25 Hz. Usually, about 40 spectra were validated for temperature calculation. Close to the injector axis, the presence of liquid oxygen led to a significant drop in validation rate due to strange spectra from LOX spray or spark from bigger

droplets. Water could be detected only at cross section 52 mm because hydrogen was our first interest and the laser system was optimized for hydrogen cross sections 87 mm and 127 mm.

MATHEMATICAL MODEL

Model

A dilute LOX spray is considered that is injected into a turbulent gaseous hydrogen stream where the inlet temperatures are cryogenic. The pressure of the system is 0.5 MPa. The model includes an Eulerian description of the gas phase and Lagrangian equations for the dilute spray. The $k-\epsilon$ turbulence model is employed where additional terms account for the interaction with the spray (Hollmann and Gutheil, 1996 and 1998). The chemical reactions are described through a flamelet model for turbulent spray diffusion flames. The conservation equations for the mixture fraction and its variance also account for mass gain through vaporization of the liquid (Hollmann and Gutheil, 1996). Complete formulation of the equations is given by Hollmann and Gutheil, 1996.

The convective heating and vaporization is described through a model developed by Abramzon and Sirignano (Abramzon and Sirignano, 1989). The equation for droplet motion accounts for turbulence effects through use of a Gaussian distribution for turbulent fluctuations (Amsden *et al.*, 1989). The total spray and its distribution is described through the discrete droplet model (Amsden *et al.*, 1989).

For the computation of the gas phase characteristics in the cryogenic temperature regime, data from JSME tables (JSME, 1983) for pressures up to 20 MPa and temperatures between 80 and 300 K are used. Moreover, the pressure (and temperature) dependence of the vaporization

rate and of the binary equilibrium composition at the liquid/gas interface (Yang *et al.*, 1994) is included.

The spray appears to be dense in the area upstream of 72 mm from the injector. Since the present study focusses on the modeling of the turbulent flame structure, the computations were started at this location which requires generation of initial profiles for the computation that are taken from the experiment.

Initial Spray Conditions

The DTV and image processing described above gives information about the size, position, and velocity of single droplets (see Fig. 4). Since it is not possible to track every single droplet in the calculation, droplets are packed into parcels which are used in the simulation (Amsden *et al.*, 1989; Schlotz, 2001). At the axial position $x = 72$ mm ten different droplet size classes $j = 1 \ldots 10$ are considered which are given in Tab. II and the radial coordinate y is divided into nine intervals $[y_i - \Delta y/2, y_i + \Delta y/2)$, $y_i = \Delta y/2 + (i-1)\Delta y$, $i = 1 \ldots 9$. At each radial position y_i the liquid mass flux $\dot{m}''_{LOX,ij}$ of LOX droplets of size class j through the volume $\Delta x \Delta y \Delta z$ is given by

$$\dot{m}''_{LOX,ij} = \left(4/3\pi\rho \sum_{n=1}^{N_{d_{ij}}} R_n^3 u_n \right) / \left(\Delta x \Delta y \Delta z \right), \tag{1}$$

where $N_{d_{ij}}$ is the number of droplets in the volume $\Delta x \Delta y \Delta z$ with $\Delta x = 4$ mm, $\Delta y = 1$ mm, $\Delta z = 0.5$ mm, R_n is the radius of droplet n and u_n its velocity in x-direction (Schlotz, 2001). (Mass fluxes in other directions are negleted.) Multiplying $\dot{m}''_{LOX,ij}$ with the ring area $A_i = 2\pi y_i \Delta y$, yields the mass flux of LOX through the ring area per time:

$$\dot{m}_{LOX,ij} = \dot{m}''_{LOX,ij} \cdot 2\pi y_i \Delta y. \tag{2}$$

The corresponding droplet rate $\dot{N}_{d_{ij}}$ through the ring area is given by

$$\dot{N}_{d_{ij}} = dN_{d_{ij}}/dt = \dot{m}_{LOX,ij} / \left(4/3\pi\rho_{LOX}\overline{R_{ij}}^3\right), \tag{3}$$

where $\overline{R_{ij}}$ is the arithmetic mean of the droplet radii at radial position y_i of the droplet size class j. At each radial position y_i the droplets are packed into $N_{p_i} = 400$ parcels. Assuming $N_{p_{ij}}/N_{p_i} = \dot{N}_{d_{ij}}/\dot{N}_{d_i}$, with $N_{p_i} = \sum_j N_{p_{ij}}$ and $\dot{N}_{d_i} = \sum_j \dot{N}_{d_{ij}}$, the distribution of the number of parcels $N_{p_{ij}}$ per size class j at radial position y_i represents the size distribution of the injected spray at every radial position y_i. So the number $N_{p_{ij}}$ is given by

$$N_{p_{ij}} = N_{p_i} \cdot \dot{N}_{d_{ij}} / \sum_j \dot{N}_{d_{ij}}. \tag{4}$$

The droplet rate for each size class at the various radial positions is shown in Fig. 5. Since not all droplets are registrated by the DTV and some droplets may already have vaporized, the total calculated mass flux

$$\dot{m}_{LOX} = \sum_{i,j} \dot{m}_{LOX,ij} \tag{5}$$

is less than the totally injected liquid mass. In the present simulation, approximately 11.1% of the total injected liquid mass is captured by the measurements.

RESULTS AND DISCUSSION

Figure 6 shows the overall structure of the spray flame in terms of the gas phase velocities. The main chemical reaction zone is located at the boundary of the spray jet where vaporized oxidizer meets the surrounding hydrogen stream. The maximum flame temperature is about 3000 K which is typical for these high-pressure flames.

A more detailed investigation of flame temperature is shown in Fig. 7 where the calculated and experimental radial profiles are shown for three different axial positions. Symbols show experimental data and lines are computational results. At $x = 72$ mm, there are no experimental data, and the inlet conditions for the gas temperature have been obtained from interpolated experimental data at two surrounding positions. Moreover, the experimental data has been extrapolated into the outer regions where no experimental data are available.

Figure 7 shows that the gas temperature in the main reaction zone is overpredicted by the computations. This may be attributed to both experimental and computational uncertainties. First the experiments employed CARS single shot measurements, and the averaging procedure of these values typically leads to an underprediction of the measured gas temperatures. Moreover, the initial gas phase profiles needed for the computations is estimated from the gas temperature profile, and this procedure is somewhat arbitrary. Another reason is to be found in the incomplete liquid phase data. The experiments usually are able to capture only up to 10–20% of the total liquid flux. The computations use the uncorrected data from measurements so that the vaporization of the neglected liquid would reduce the gas phase temperature. Therefore, the discrepancies of computed and measured temperature profiles in the gas phase is reasonable. Another source of uncertainties in the computations is the unknown gas species profiles. Their initial conditions need to be estimated for the computation. Here, stoichiometric mixture is assumed at the peak gas temperature, and these values are extrapolated into the colder regions of the flame taking into account the boundary conditions of these variables. This procedure may also result in an overprediction of computed gas phase temperatures. In a future experimental study, the gas phase species profiles will be investigated.

The flamelet model is suitable to predict all species profiles that are considered in the

laminar flamelet library. Figure 8 shows radial profiles at $x = 127$ mm. The HO_2 and H_2O_2 are present in the colder flame region (due to their stability) on the air side of the flame, and the location of the H_2O peak is shifted to the fuel side which is typical for gas phase combustion. Details of the laminar flame structures that are used for the present computations are given by Schlotz and Gutheil, 2000.

Figures 9 and 10 show a comparison of liquid phase characteristics. Figure 9 displays the radial profile of the Sauter mean radius at $x = 104$ mm. Symbols show experimental results, and the agreement between experiment and computation is excellent. The same is true for the profiles of axial velocities at the same axial position shown in Fig. 10. Thus it is shown that the present model is suitable to correctly predict the liquid phase properties. The experiment reveals a recirculation zone of the gas phase velocity which is also captured by the computations shown in Fig. 11.

SUMMARY AND FUTURE RESEARCH

The combustion process in the micro combustion chamber M3 has been studied by both experimental methods and numerical computations. The Eulerian/Lagrangian model is suitable to predict the processes in the dilute spray regime of the combustion chamber. In particular, the prediction of the spray distribution and evolution is very good.

Calculated gas phase temperatures are higher than the experimental values which is explained by various reasons. First, the experimental data are somewhat underpredicted which is typical for CARS single shot measurements. Moreover, only a small portion of the total liquid flux was captured by the experimental techniques so that the energy consumed by droplet

vaporization is underpredicted leading to too high values of gas temperature.

Future studies should include the dense spray regime, and an extension of the present model into that region will be developed. The experiment will address measurements of the gas phase species in presence of droplets which will improve both the fromulation of initial conditions for the computations as well as the comparison with results from the flamelet model for turbulent spray flames.

ACKNOWLEDGEMENTS

Financial support through the DARA and TEKAN projects as well as the Deutsche Forschungsgemeinschaft through SFB 359 is gratefully acknowledged.

REFERENCES

Abramzon, G. and Sirignano, W. A. (1989) Droplet vaporization model for spray combustion calculations. *Int. J. Heat Mass Transfer*, 9: 1605–1618.

Adrian, R. J. (1991) Particle-imaging techniques for experimental fluid mechanics. *Annual Review of Fluid Mechanics*, 23: 261–304.

Amsden, A. A., O'Rourke, P. J., Butler, T. D. (1989) KIVA II, a computer program for chemically reactive flows with sprays. *Los Alamos National Laboratory Report LA-11560-MS*, UC-96.

Balakrishnan, G. (1993) Studies of hydrogen-air diffusion flames and of compressibility effects related to high-speed propulsion. *Ph.D. Thesis*, University of California San Diego, CA, USA.

Brummund, U., Vogel, A., Oschwald, M., Grisch, F., Bouchardy, M., Pealat, M., Vingert, L., Candel, S., Herding, G., Scouflaire, P., Snyder, R., Rolon, C. (1995) Laser diagnostics for cryogenic propellant combustion studies. *2nd International Symposium on Liquid Rocket Propulsion*, ONERA–Chatillon, France.

Clauß, W., Kozlov, D. N., Pykhov, R. L., Smirnov, V. V., Stel'makh, O. M., Vereshagin, K. A. (1997) The Analysis of the Precision of Single Shot 2l-CARS Temperature Measurements in Hydrogen, *Appl. Phys.*, **65**:619–624.

Eckbreth, A. C. (1996) *Laser diagnostics for combustion temperature and species*, 2nd Ed., Gordon and Breach, Combustion science and technology book series.

Hollmann, C. and Gutheil, E. (1998) Flamelet–modeling of turbulent spray diffusion flames based on laminar spray flame library. *Combust. Sci. and Tech.*, 135: 175–192.

Hollmann, C. and Gutheil, E. (1996) Modeling of turbulent spray diffusion flames including detailed chemistry. *Proc. Comb. Inst. 26(1)*, 1731–1738.

JSME Data Book (1983) Thermophysical Properties of Fluids.

Schlotz, D. (2001) Modellierung laminarer und turbulenter Flüssig-Sauerstoff/Wasserstoff-Sprayflammen unter kryogenen Hochdruckbedingungen. *Ph.D. Thesis*, Stuttgart University.

Schlotz, D. and Gutheil, E. (1999) Modeling of laminar mono– and bidispers LOX/H_2 spray flames for cryogenic conditions. *15th Annual Conference on Liquid Atomization and Spray Systems*, July 5–7, Toulouse, France.

Schlotz, D. and Gutheil, E. (2000) Modeling of laminar mono– and bidisperse liquid oxygen/hydrogen sprayflames in the counterflow configuration. *Combust. Sci. and Tech.*, 158: 195–210.

Sender, J., Lecourt, R., Oschwald, M., Haidn, O. J. (1997) Application of droplet-tracking-velocimetry to LOX/GH_2 coaxial-spray combustion with varying combustion chamber pressures. *Proceedings of the 13th Annual Conference on Liquid Atomization on Spray Systems*, Florence, Italy, 145–154.

Smirnov, V. V, Clauß, W., Oschwald, M., Grisch, F., Bouchardy, P. (2000) Theoretical and practical Issues of CARS application to cryogenic spray combustion, *4th International Symposium ob Liquid Space Propulsion*, Heilbronn, March 13-15.

Warnatz, J., Maas, U., Dibble, R. W. (1996) *Combustion*, Springer, Heidelberg.

Yang, V., Lin, N. N., Shueb, J.S. (1994) Vaporization of liquid oxygen (LOX) droplets in supercritical hydrogen environments. *Comb. Sci. and Tech.*, 97: 247–270.

List of Tables

List of Figures

Table I: Operating conditions and typical parameters test case 0.5 MPa

p_c [MPa]	$\dot{m}_{O_2}$ [g/s]	$\dot{m}_{H_2}$ [g/s]	v_{O_2} [m/s]	v_{H_2} [m/s]	W $\cdot 10^{-3}$	J [-]	Re_{O_2} $\cdot 10^{-5}$	r_{of} [-]	V_{fo} [-]
0.5	39	5.5	24	426	20.0	0.61	1.47	7.1	17.7

Table II: Range of radii R of the ten droplet size classes in μm.

j	1	2	3	4	5	6	7	8	9	10
R	$[0, 5]$	$(5, 10]$	$(10, 15]$	$(15, 20]$	$(20, 25]$	$(25, 30]$	$(30, 37.5]$	$(37.5, 45]$	$(45, 52.5]$	$(52.5, 60]$

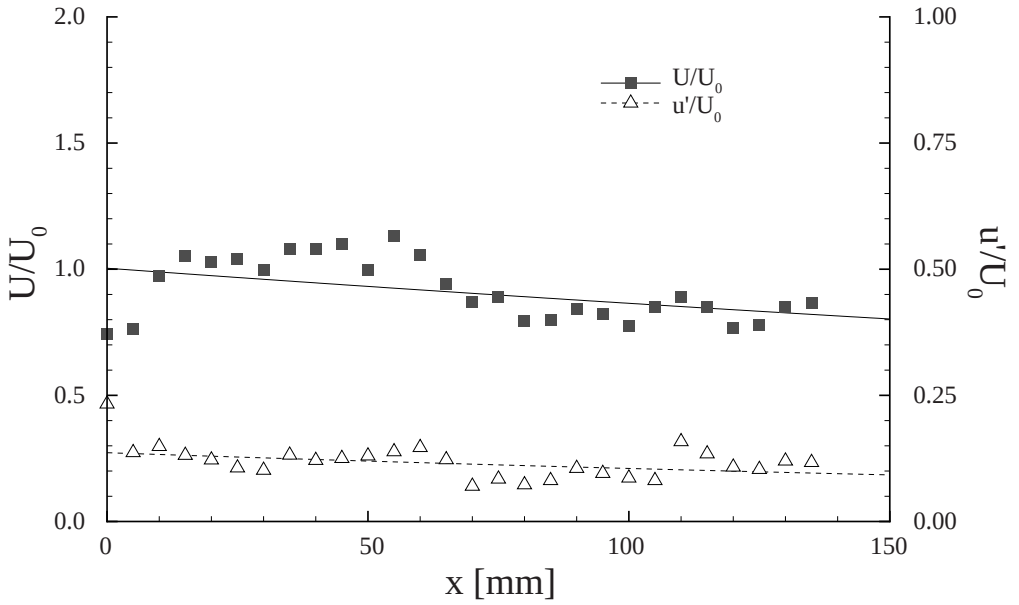

Figure 1: Velocity distribution at p_c=0.5 MPa.

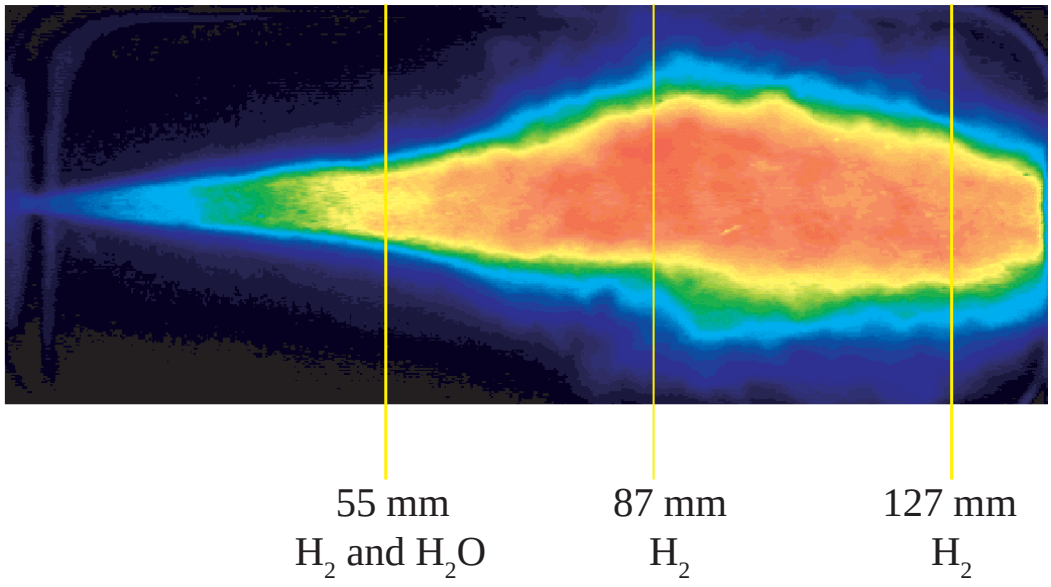

Figure 2: Flame inside the combustion chamber with CARS measurement positions.

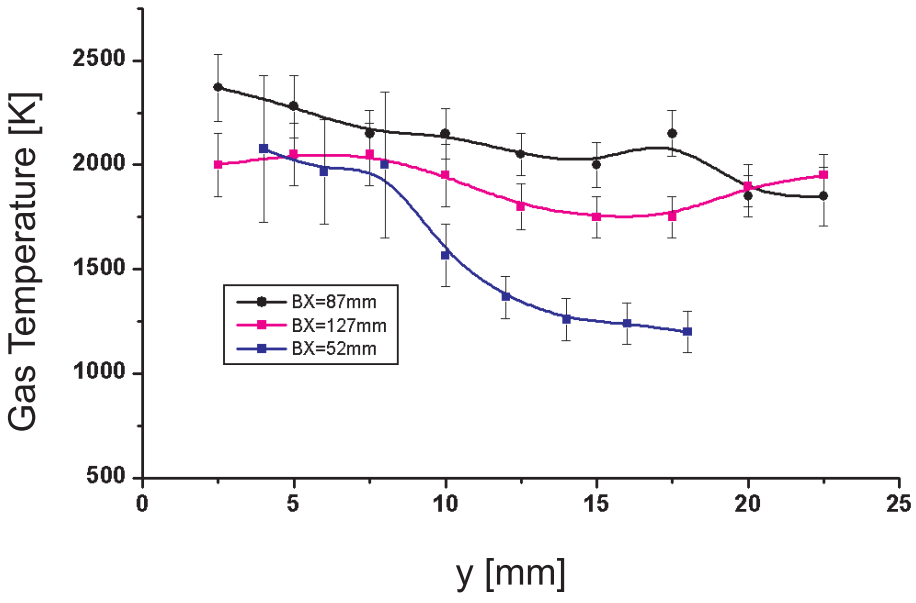

Figure 3: Hydrogen–CARS temperatures mean values at different positions.

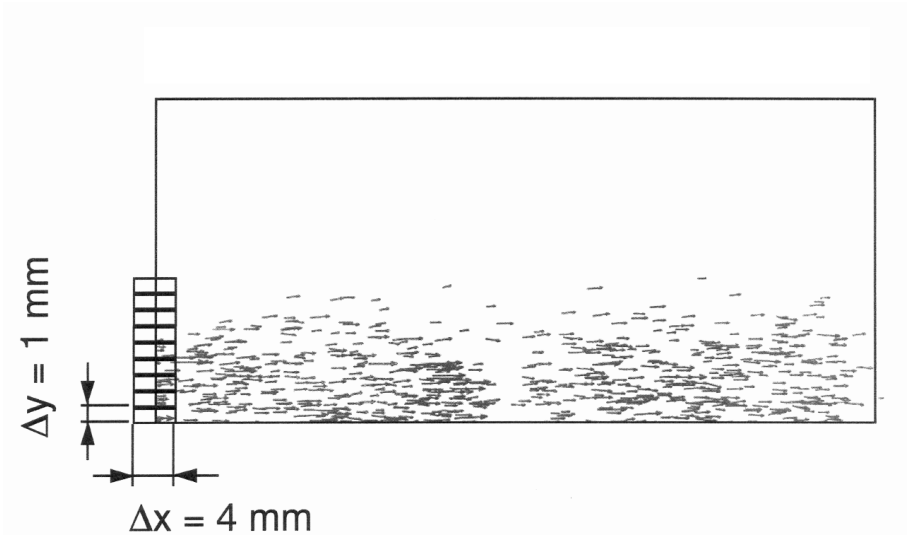

Figure 4: Droplet size and velocity measurements using particle image velocimetry in the range of 72 mm and 140 mm.

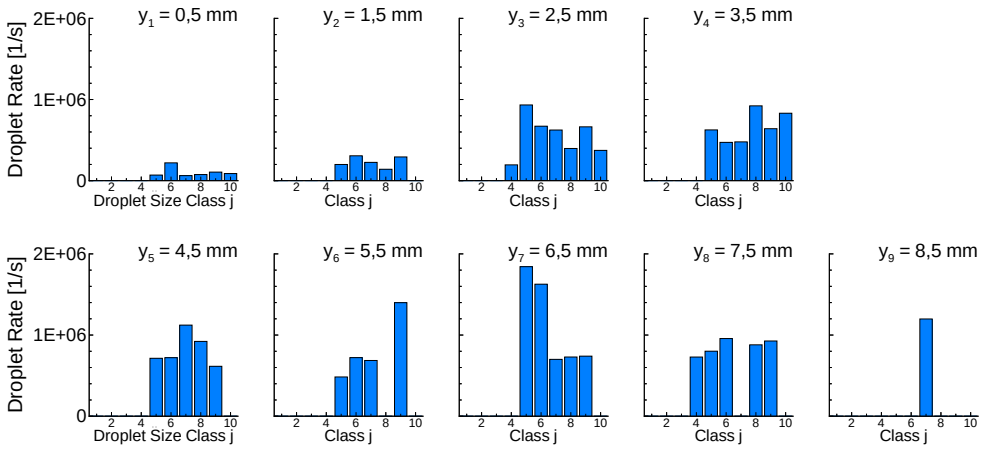

Figure 5: Droplet rate as a function of the droplet size class j and the radial position y_i.

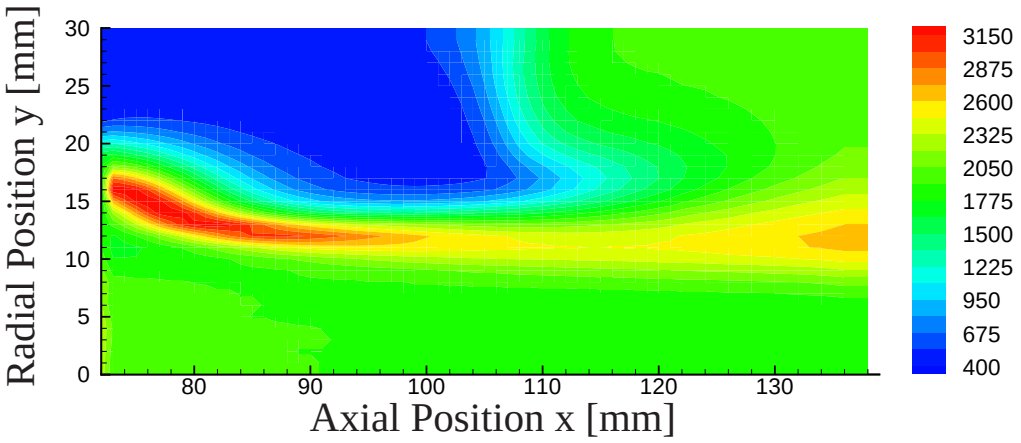

Figure 6: Contour plot of the gas temperature

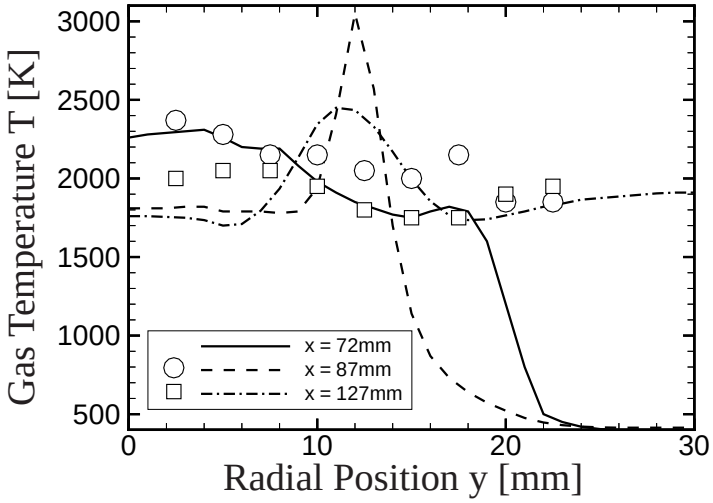

Figure 7: Radial profiles of the gas temperature for three different axial positions: Symbols present experimental data and lines show computational results.

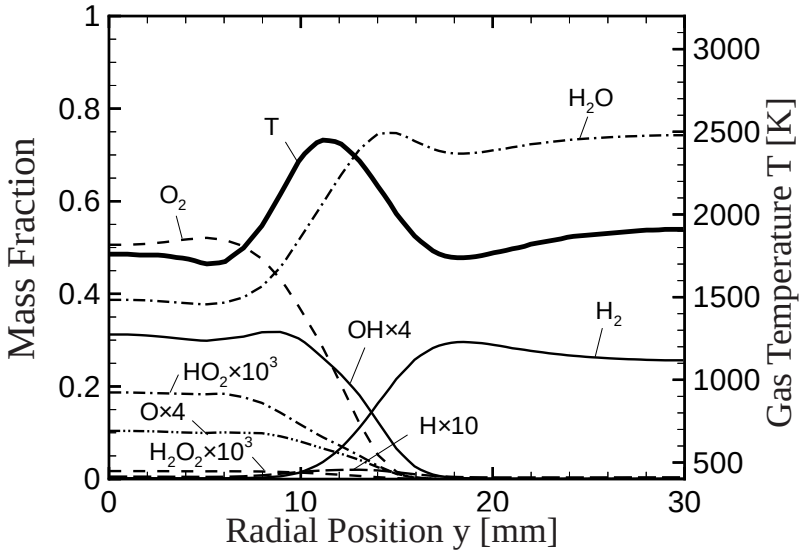

Figure 8: Radial profiles of the gas temperature and species mass fractions at $x = 127$ mm.

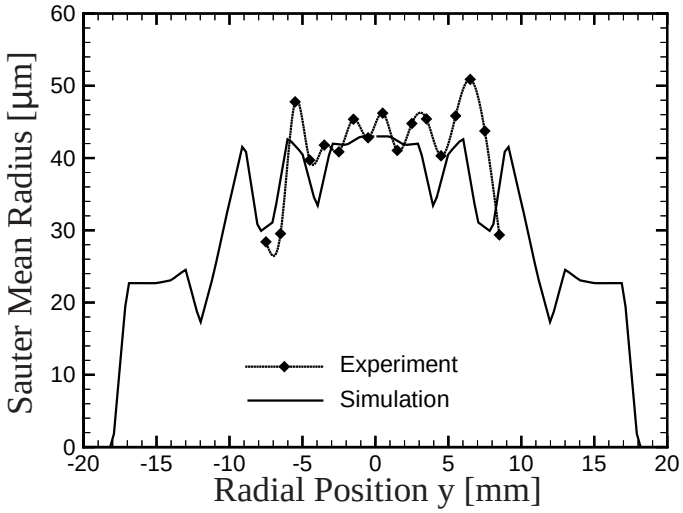

Figure 9: Experimental and computational results of the Sauter mean radius at $x = 104$ mm.

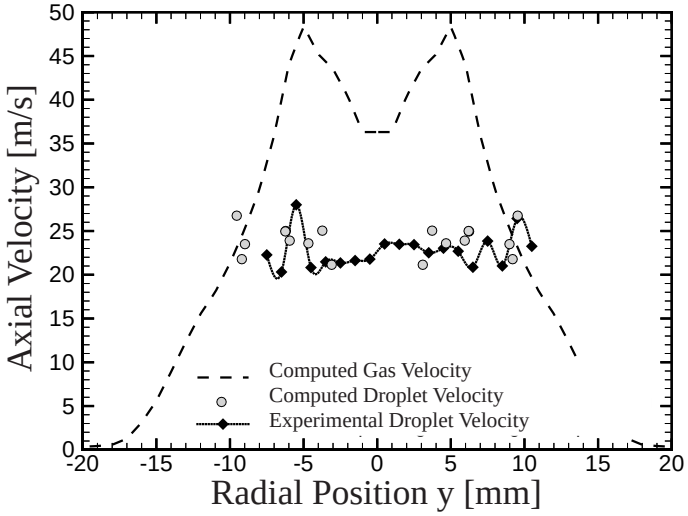

Figure 10: Experimental and computational results of the droplet velocities as well as calculated gas velocities at $x = 104$ mm.

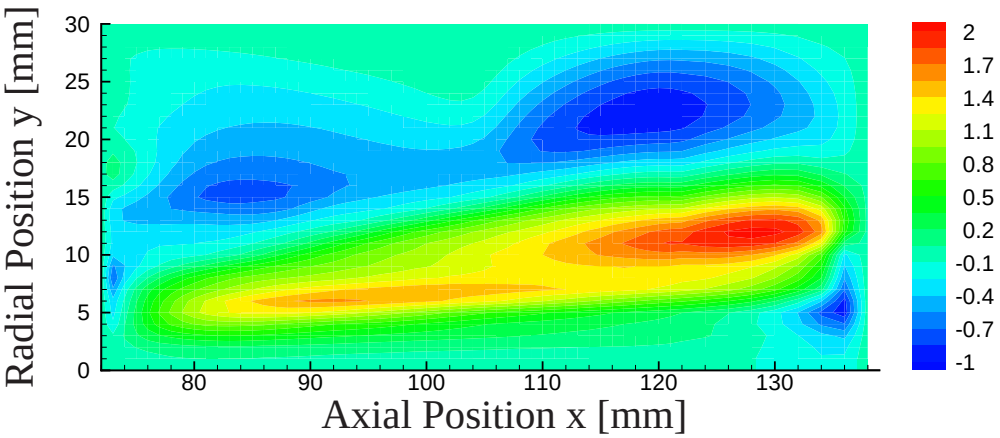

Figure 11: Contour plot of the computed radial gas velocity.